Dendrochronologia 50 (2018) 81–90

Contents lists available at ScienceDirect

Dendrochronologia

journal homepage: www.elsevier.com/locate/dendro

Large-scale, millennial-length temperature reconstructions from tree-rings

Jan Esper[a,*], Scott St. George[b], Kevin Anchukaitis[c], Rosanne D'Arrigo[d], Fredrik Charpentier Ljungqvist[e,l,k], Jürg Luterbacher[f], Lea Schneider[f], Markus Stoffel[g,h,i], Rob Wilson[j], Ulf Büntgen[k]

[a] Department of Geography, Johannes Gutenberg University, Mainz, Germany
[b] Department of Geography, Environment and Society, University of Minnesota, Minneapolis, USA
[c] School of Geography and Development, University of Arizona, Tucson, AZ, USA
[d] Lamont-Doherty Earth Observatory of Columbia University, Palisades, NY, USA
[e] Department of History, Stockholm University, Stockholm, Sweden
[f] Department of Geography, Justus Liebig University, Giessen, Germany
[g] Institute for Environmental Sciences, University of Geneva, Geneva, Switzerland
[h] Department of Earth Sciences, University of Geneva, Geneva, Switzerland
[i] Department F.-A. Forel for Aquatic and Environmental Sciences, University of Geneva, Geneva, Switzerland
[j] School of Geography and Geosciences, University of St Andrews, UK
[k] Department of Geography, University of Cambridge, Cambridge, UK
[l] Bolin Centre for Climate Research, Stockholm University, Stockholm, Sweden

ARTICLE INFO

Keywords:
Tree-ring width
Maximum latewood density
Warm season temperatures
Medieval Warm Period
Little Ice Age
Northern Hemisphere

ABSTRACT

Over the past two decades, the dendroclimate community has produced various annually resolved, warm season temperature reconstructions for the extratropical Northern Hemisphere. Here we compare these tree-ring based reconstructions back to 831 CE and present a set of basic metrics to provide guidance for non-specialists on their interpretation and use. We specifically draw attention to *(i)* the imbalance between (numerous) short and (few) long site chronologies incorporated into the hemispheric means, *(ii)* the beneficial effects of including maximum latewood density chronologies in the recently published reconstructions, *(iii)* a decrease in reconstruction covariance prior to 1400 CE, and *(iv)* the varying amplitudes and trends of reconstructed temperatures over the past 1100 years. Whereas the reconstructions agree on several important features, such as warmth during medieval times and cooler temperatures in the 17th and 19th centuries, they still exhibit substantial differences during 13th and 14th centuries. We caution users who might consider combining the reconstructions through simple averaging that all reconstructions share some of the same underlying tree-ring data, and provide four recommendations to guide future efforts to better understand past millennium temperature variability.

1. Introduction

Anthropogenic greenhouse gases are currently the dominant climate forcing on our planet, but that fact does not imply that natural forcings such as volcanic eruptions and solar variability will no longer be important. Reconstructing pre-Anthropocene (Crutzen, 2002) climate variability is therefore of critical importance to improve our understanding of the complex interactions within the Earth's climate system and to reduce uncertainties in projecting future climate change using model simulations. This requirement is not only relevant for climate variations over the past million years during which several kilometer-thick continental ice-sheets developed, and sea level changed by more than 100 m (Liedtke, 1981; Rohling, 2017; Siddall et al., 2003), but is arguably even more important for the past 1000 years, with its prolonged temperature changes between the Medieval Warm Period (MWP) and Little Ice Age (LIA) (Lamb, 1972). An accurate reconstruction of these largely naturally forced climate variations, including an improved understanding of the course and amplitude of temperature variability at continental to hemispheric scales, has been a central research objective for the paleoclimate community during the past two decades (Luterbacher et al., 2016; Pages 2k Consortium, 2013).

Efforts to reconstruct Southern Hemisphere (SH), Northern Hemisphere (NH), and even global mean temperatures have been plentiful and include estimates based on only tree-rings as well as combinations of different archives, so-called multi-proxy

* Corresponding author.
E-mail address: esper@uni-mainz.de (J. Esper).

https://doi.org/10.1016/j.dendro.2018.06.001
Received 7 April 2018; Received in revised form 31 May 2018; Accepted 4 June 2018
Available online 11 June 2018

Table 1
Tree-ring based large scale temperature reconstructions.

Reconstruction	Acronym	Objective	Network characteristic	Comment
Briffa (2000) (QSR)	Bri00	First representation of NH high latitude summer temperatures of the past millennium	Combines a limited number of site chrono-logies from 45-72 °N	Network mean not calibrated against instr. temperatures
Esper et al. (2002) (Science)	Esp02	Preserving low frequency trends in NH extratropical temperature reconstruction	Includes site chronologies with weak temperature signals	Variance stabilized and calibrated in Frank et al. (2007a,b)
D'Arrigo et al. (2006) (JGR)	DAr06	Representation of NH extratropics using best-calibrating site chronologies	Includes many shorter chronologies covering the past few centuries	Divergence between tree-rings and temperatures noted
Schneider et al. (2015) (GRL)	Sch15	Retaining high frequency, post-volcanic cooling signals	Combines only long MXD chronologies	14th century warmer than in any other reconstruction
Stoffel et al., 2015 (NatGeo)	Sto15	Representation of NH extratropics including post-volcanic cooling signals	Includes many new TRW and MXD chronologies	Shows stronger post-volcanic cooling than other record
Wilson et al. (2016) (QSR)	Wil16	Improved representation of NH extratropics using best-calibrating site chronologies	New chronologies plus PC-derived grid point "chronologies" in Asia	Spatially resolved reconstruction in Anchukaitis et al. (2017)

reconstructions (see reviews by Christiansen and Ljungqvist, 2017; Frank et al., 2010; Jones et al., 2009; Smerdon and Pollack, 2016). Important multi-proxy temperature reconstructions have been produced by Neukom et al. (2014) for the SH, Christiansen and Ljungqvist (2011), 2012; Crowley and Lowery (2000); Hegerl et al. (2007); Juckes et al. (2007); Ljungqvist (2010); Mann et al. (1999); Moberg et al. (2005); Shi et al. (2013) for the NH, and Jones et al. (1998); Loehle (2007); Mann and Jones (2003); Mann et al. (2008) at the global scale. The integration of multiple archives is challenging, however, as only tree-rings provide precise annual dating control over the entire past millennium (and a few documentary records from Europe and Asia; Qian et al., 2003; van Engelen et al., 2001) and can be rigorously calibrated and verified against instrumental temperature data (Cook et al., 1994). Millennial-length temperature reconstructions that are solely sourced from tree-rings include work by Briffa (2000); Esper et al. (2002); D'Arrigo et al. (2006); Schneider et al. (2015); Stoffel et al. (2015), and Wilson et al. (2016), all covering larger fractions of the Northern Hemisphere extratropics (Table 1). Another recently published NH reconstruction from only tree-rings is not included here as the record lacks annual resolution (Xing et al., 2016). The representation of SH temperatures is generally more challenging because of the sparsity of land masses and limited number of records from terrestrial archives (Neukom and Gergis, 2012). There are currently only four tree-ring based local temperature reconstructions covering the past millennium available from the SH (Esper et al., 2016) precluding the development of purely dendro-based reconstructions for that hemisphere.

The first attempt of combining millennial-length tree-ring chronologies to represent temperatures at large spatial scales was accomplished almost 20 years ago when Keith Briffa averaged seven tree-ring width (TRW) and two maximum latewood density (MXD) chronologies from high latitude sites in Eurasia and North America (Briffa, 2000; hereafter Bri00) (Table 1). The network mean was later regressed against annual temperatures from 1881 to 1960 (Briffa and Osborn, 2002) and displayed in various publications and IPCC assessment reports. This pioneering work was subsequently complemented by the development of a larger network integrating 14 TRW site chronologies (Esper et al., 2002; hereafter Esp02), in which the authors particularly emphasized long-term trends in response to the relatively flat pre-instrumental temperature history displayed by the iconic "hockey stick" multi-proxy reconstruction (Mann et al., 1999). The variance of the Esp02 network mean was later adjusted for changes in tree replication and formally calibrated against annual land temperatures averaged over 20–90 °N (Frank et al., 2007b). Another milestone was the development of a 20–90 °N temperature reconstruction extending back to 747 CE integrating many more, also shorter, TRW chronologies with the objective to best represent the spatial domain of the NH extratropics (D'Arrigo et al., 2006; hereafter DAr06). DAr06 also identified an offset between warming late 20th century temperatures and (less increasing) tree-ring values in parts of their network, the so-called divergence problem (Briffa et al., 1998; D'Arrigo et al., 2008; Esper and Frank, 2009) questioning the skill of tree-ring data to properly reproduce temperatures during pre-instrumental warm periods, such as the MWP. About 10 years later, three new reconstructions of NH extratropical temperatures were published, including a purely MXD based record by Schneider et al. (2015; hereafter Sch15), and two records combining many more site chronologies than any previous attempt (Stoffel et al., 2015; Wilson et al., 2016; hereafter Sto15 and Wil16, respectively). Whereas Sch15 and Wil16 both aimed to reproduce temperature variability at all timescales, Sto15 was designed for the analysis of short term summer cooling patterns following large volcanic events. Wil16 combined published TRW and MXD chronologies expressing good calibration against instrumental data and starting prior to 1750 to best represent warm season temperatures from 40 to 75 °N (Table 1).

Here we assess these six millennial-length temperature reconstructions from tree-rings to facilitate their use by colleagues from other disciplines. We focus on the large-scale mean timeseries as these are the prime products reused in other work, though acknowledge the importance of spatially resolved reconstructions (Anchukaitis et al., 2017; Guillet et al., 2017) for multiple scientific applications including proxy-model assessments (Bothe et al., 2015; Fernández-Donado et al., 2013; Hartl-Meier et al., 2017; Ljungqvist et al., 2016). We analyze the changing numbers of tree-ring series (replication) included in the reconstructions, evaluate the reconstructions' climate signals and covariance, and compare the reconstructed temperatures over their common period since 831 CE considering basic metrics. We conclude by providing four recommendations to support an improved understanding of pre-instrumental temperature variability over the past millennium at regional to hemispheric scales.

2. Sample size

Although the six large-scale temperature reconstructions are derived from different sets of tree-ring networks, all of them share some of the same data. The older reconstructions (Bri00, Esp02) utilized smaller networks compared to the newer ones, largely because fewer tree-ring chronologies were available at that time and the authors focused more rigorously on the inclusion of only long chronologies. An exception from this tendency is Sch15, who combined a limited number of long MXD chronologies, thereby restricting the spatial representation compared to DAr06 and particularly Sto15 and Wil16. Besides the shift towards larger tree-ring networks, some sites have been used in every reconstruction. A prime example is the Torneträsk MXD chronology from northern Sweden that was originally published in 1988 (Schweingruber et al., 1988) and thereafter has been updated and changed (Grudd, 2008; Melvin et al., 2013). The newer Torneträsk versions integrate more density data, though the core of MXD series from relict material remained the same (Esper et al., 2014). Such gradual changes and improvements of site chronologies, and the integration of different versions of these local records in the hemispheric

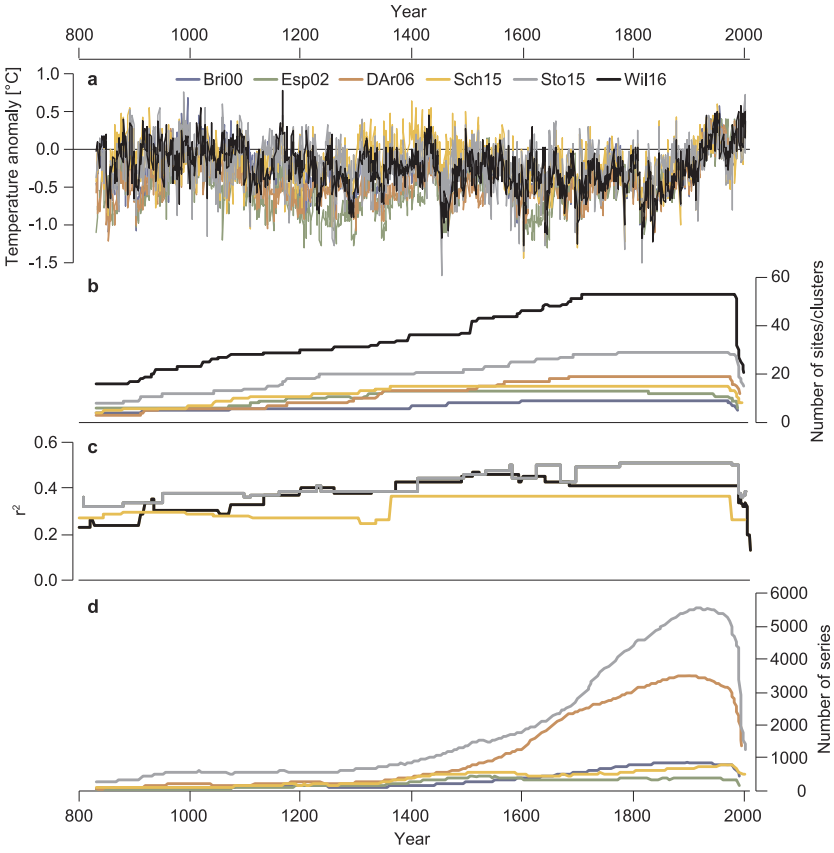

Fig. 1. Millennial-length temperature reconstructions from tree-rings. **a,** Six warm season temperature reconstructions of larger fractions of the Northern Hemisphere reaching back to 831 CE. All records are scaled against 30–70 °N JJA temperatures over the common 1881–1992 period, and expressed as anomalies from 1961-1990. **b**, The temporally changing number of site chronologies (Bri00, Esp02, Sch15) and regional clusters (DAr06, Sto15, Wil16) combined in the large-scale reconstructions. **c**, r^2 statistics of the differently replicated nests of the recently published Sch15, Sto15 and Wil16 reconstructions. **d**, The temporally changing number of measurement series (trees or stem radii) combined in the reconstructions (data for Wil16 cannot be reproduced).

networks, complicate the comparison of replication changes among the large-scale reconstructions. In addition, a proper differentiation between numbers of measurement series and numbers of trees is not feasible at the hemispheric scale. This is because the practices of sampling trees (e.g. one or multiple cores per tree) and chronology development (e.g. calculating tree mean curves or forwarding radii series) change among sites and research groups, and are often incompletely documented, particularly for the sites sampled in the 1970 s–1990 s.

When assessing reconstruction replication, we need to differentiate between three levels of data aggregation: “site chronologies”, “regional clusters”, and “grid point chronologies” (Fig. 1). A site chronology is the mean of a number of measurement series (MXD or TRW) from an ecologically coherent environment, such as the area surrounding Lake Torneträsk in northern Sweden. Site chronologies are the classic unit used and combined in Bri00 (#9 chronologies), Esp02 (#14) and Sch15 (#15), although the situation is already nontrivial in Bri00, for example, as both a TRW and (shorter) MXD chronology were used from Torneträsk as well as Yamal (northwestern Siberia). Regional clusters represent the combination of several site chronologies of differing length from a larger area such as the European Alps (integrating #10 chronologies) or northwestern Alaska (#4) in DAr06, for example. Cluster mean curves were introduced by DAr06 (#19 clusters) and used by Sto15 (#30) and Wil16 (#54; Fig. 1b). They also form the basis for the calculation of calibration statistics in the state-of-the-art reconstructions, including the explained variance of instrumental temperature variability (r^2) echoing the change in cluster replication: r^2 declines back in time as the longer nests integrating fewer cluster means explain less temperature variance (Fig. 1c). The numbers of underlying (TRW or MXD) measurement series are apparently much larger in cluster means than in chronologies, but in both cases, it is still evident which specific sites are included in a given cluster. That information is not available for grid point chronologies, as additionally used in Wil16 from 18 locations in central and eastern Asia. The grid point chronologies were originally produced by Cook et al. (2013) using principal component regression. While consideration of these additional data points allowed the inclusion of an otherwise underrepresented area in Wil16, it comes at the cost of losing the ability to represent the numbers of included measurement series.

Keeping these restrictions in mind, we traced the replication of each network back to the numbers of measurement series (except for Wil16 using grid point chronologies) but acknowledge that we are not able to differentiate between trees and radii (Fig. 1d). Overall, the numbers of trees integrated in the large-scale networks has increased substantially since the early work by Bri00. The 19 regional clusters in DAr06 are composed of 66 site chronologies including > 3400 series (trees or cores) during the late 19th century, and the 30 clusters in Sto15 are composed of 233 site chronologies including > 5500 series during the early 20th century. In comparison, the earlier Bri00 and Esp02 networks, but also the purely MXD based Sch15 network, integrate much fewer series and do not exceed 900 at any time of the last millennium. Replication in these smaller networks also declines to only 132 series in Sch15, 74 series in Esp02, and 119 series in Bri00 during the 11th century, substantially limiting the ability to represent temperatures during the MWP compared to the 20th century calibration period. Eleventh century replication is improved in DAr06 (187 series) and particularly Sto15 (569 series), but the general imbalance between fewer series covering the full millennium and numerous series covering the past few centuries remains. This situation is likely similar for Wil16, except that even more tree-ring series are included in this network, which is the most comprehensive of all examples.

3. Signal strength

We re-calibrated all tree-ring based reconstructions against June-August temperatures averaged over 30–70 °N land areas (Harris et al., 2014), but acknowledge that the results would slightly change if an extended warm season (e.g. May–September) or different area (e.g. 30–80 °N) were considered (not shown). Using annual mean

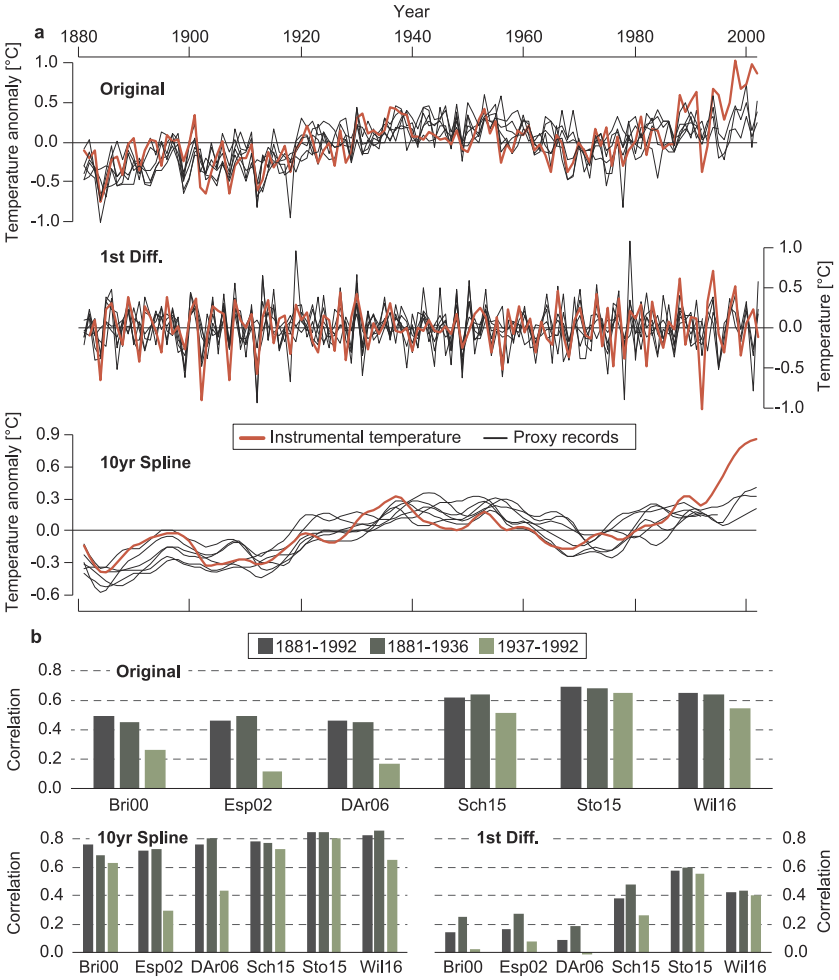

Fig. 2. Reconstruction calibration. **a**, Six large-scale temperature reconstructions (black) scaled over the 1881–1992 common period against JJA instrumental temperatures averaged over 30–70 °N land areas (red). Top panel shows the original timeseries, middle panel the timeseries after first differencing, and bottom panel the timeseries after 10-year low pass filtering. Bri00 and Esp02 end in 1992, DAr06 in 1995, and Sch15, Sto15 and Wil16 in 2002. **b**, Correlation between the tree-ring based reconstructions and instrumental JJA temperatures over the full (1881–1992; dark green), early (1881–1936; green), and late (1937–1992; light green) calibration periods. Top panel shows the results of the original series, bottom left panel of the 10-year smoothed series, and bottom right panel of the first differenced series.

temperatures, as was done in the earlier papers (Bri00, Esp02, DAr06) is inadvisable, as the trees of almost all sites included in the networks react most sensitive to warm season temperatures (Anchukaitis et al., 2017). We calculated Pearson correlations over the common period of overlap between proxy and instrumental data (1881–1992), as well as an early (1881–1936) and late (1937–1992) calibration period, and considering the original, high-pass and 10-year low pass filtered (proxy and instrumental) data to assess signal strength changes in different frequency domains (Fig. 2). Instrumental data prior to 1881 are not considered here, as the early warm season temperatures were shown to be biased by direct or reflected radiation due to insufficient sheltering (Böhm et al., 2001, 2010; Frank et al., 2007a; Parker, 1994).

The tree-ring based reconstructions calibrate differently against instrumental temperatures, with the newer records (Sch15, Sto15, Wil16) performing substantially better particularly in the high frequency domain and towards the second half of the 20th century. Whereas the recently published reconstructions all correlate $r > 0.62$ against summer temperatures (1881–1992), none of the older reconstructions (Bri00, Esp02, DAr06) exceeds $r = 0.49$. This difference is even more striking over the recent 1937–1992 calibration period, during which the older reconstructions do not explain more than 7% temperature variance ($r = 0.26$; minimum in Esp02 = 0.12) revealing a substantial loss of signal strength during the 20th century. This signal deterioration is largely mitigated, if not overcome, by Sch15, Sto15, and Wil16, even though a positive deviation of instrumental summer temperatures in the 1990 s and early 2000 s is visible in the original and low-pass filtered reconstructions (top and bottom panels in Fig. 2a). This post-1990 divergence, however, coincides with a decline in chronology and series replication in all reconstructions, as is also reflected in the r^2 statistics of Sch15, Sto15 and Wil16 (Fig. 1b–d).

All six reconstructions correlate well with the 10-year smoothed instrumental data ($r_{1881–1992} = 0.71$-0.84), which demonstrates the skill of tree-ring data to retain low frequency summer temperature variability (Fig. 2b). This signal appears to be fairly robust between the early and late calibration periods, except to DAr06 and Esp02 for which the correlations decline to $r = 0.44$ and 0.29 during 1937–1992, respectively. The situation is entirely different with the first differenced data, however, as only the recently published Sch15, Sto15 and Wil16 reconstructions reveal some skill ($r_{1881–1992} = 0.38$-0.58), whereas the early Bri00, Esp02 and DAr06 records all correlate $r < 0.17$. The overall superior calibration of the recently published reconstructions, and particularly their improved correlation in the high frequency domain, are the result of *(i)* the better replicated chronology networks and *(ii)* the use of more MXD chronologies. The latter typically calibrate better against instrumental temperatures (compared to TRW) and are less biased by biological memory effects (Büntgen et al., 2015; Briffa et al., 1998; D'Arrigo et al., 2013; Esper et al., 2015; Frank and Esper, 2005). While all first differenced reconstructions correlate weaker during the recent 1937–1992 period, the high frequency signal completely disappears in the older Bri00, Esp02 and DAr06 reconstructions, reinforcing that these early attempts should not be used for assessments of year-to-year variations in climate, in particular the response to volcanic eruptions (Anchukaitis et al., 2012).

The addition of more MXD chronologies into the latest tree-ring networks also reduces reconstruction memory so that the lag-1 autocorrelations of Wil16 ($r_{lag\text{-}1} = 0.61$), Sch15 (0.46) and particularly Sto15 (0.23) are smaller and more realistic compared to the earlier reconstructions ($r_{lag\text{-}1} = 0.67$-0.80) over the 1881–1992 common

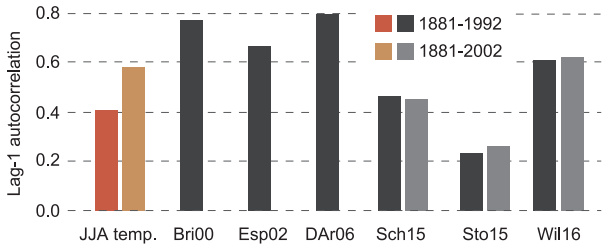

Fig. 3. Reconstruction memory. Lag-1 autocorrelation of 30-70° mean JJA land temperatures and large-scale reconstructions over the common period 1881–1992 (red and black) and extended period 1881–2002 (orange and grey).

period of overlap with instrumental data (Fig. 3). Whereas the older reconstructions overestimate the autocorrelation of the target instrumental data, the purely MXD based Sch15 reconstruction matches the first-order memory of the large-scale (30–70 °N) temperature record quite closely. The memory in the instrumental record increases substantially (from 0.41 to 0.59) if lag-1 autocorrelations are calculated over the extended 1881–2002 period covered by the recently published reconstructions (orange bar in Fig. 3). This change is largely driven by the rapid increase in summer temperatures since the late 20th century (Fig. 2a), resulting in a closer match between the temperature and Wil16 autocorrelations over the 1881–2002 period. The Sto15 reconstruction, however, undershoots the target data autocorrelation, potentially indicating an overestimation of variance in the high frequency domain at this large spatial scale.

4. Reconstruction variance and covariance

The calculation of 100-year running standard deviations reveals periods of changing reconstructed temperature variance over the past millennium (Fig. 4). Periods of increased variance have been shown to coincide with severe post-volcanic cooling events that synchronize temporal variance changes between continental scale temperature reconstructions and model simulations (Hartl-Meier et al., 2017). The six large-scale reconstructions evaluated here display substantial standard deviation changes ranging from 0.14 °C during 1303–1402 in DAr06 to 0.38 °C during 1535–1634 in Esp02 (the orange and green curves in Fig. 4a). The reconstructions are characterized by simultaneous

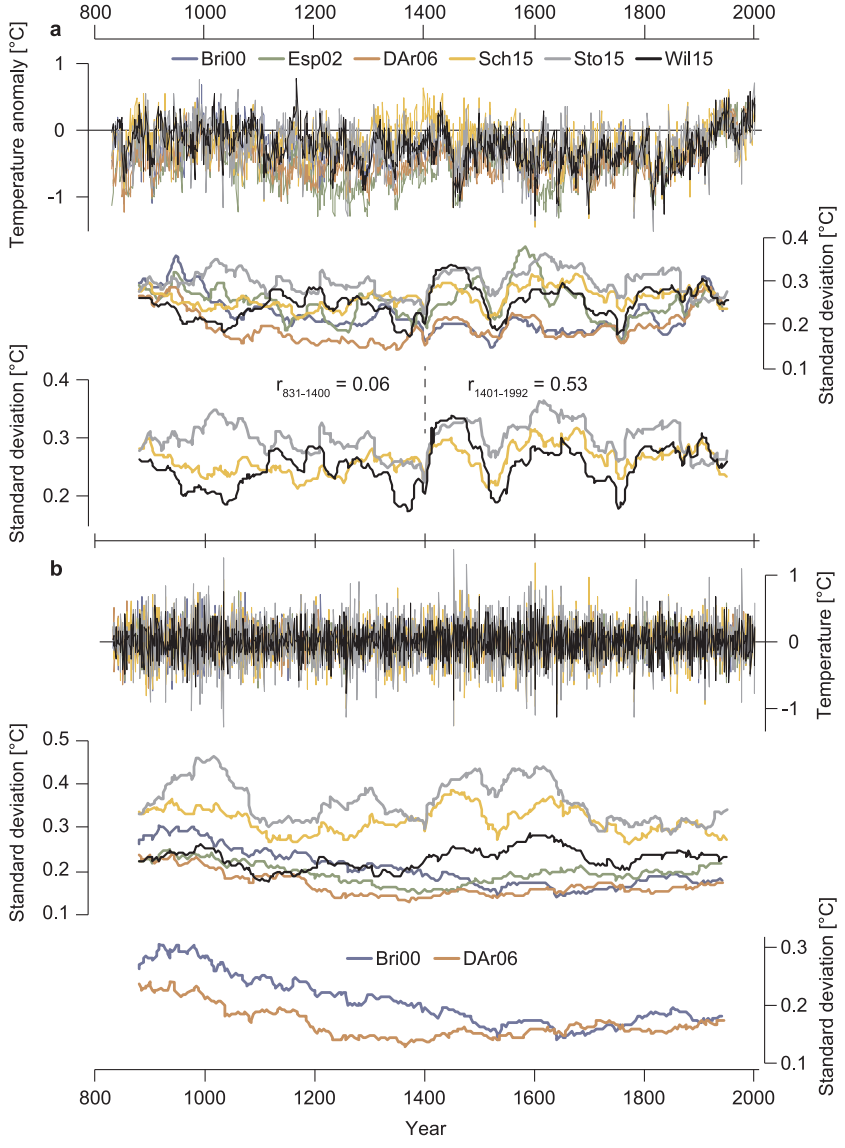

Fig. 4. Reconstruction variance. **a**, Tree-ring based temperature reconstructions (top panel) and their 100-year running standard deviation curves (middle panel). Bottom panel highlights the running standard deviations of the recently published Sch15, Sto15 and Wil16 records. **b**, Same as in **a**, but for the first differenced reconstructions. Bottom panel highlights the running standard deviations of the Bri00 and DAr06 records.

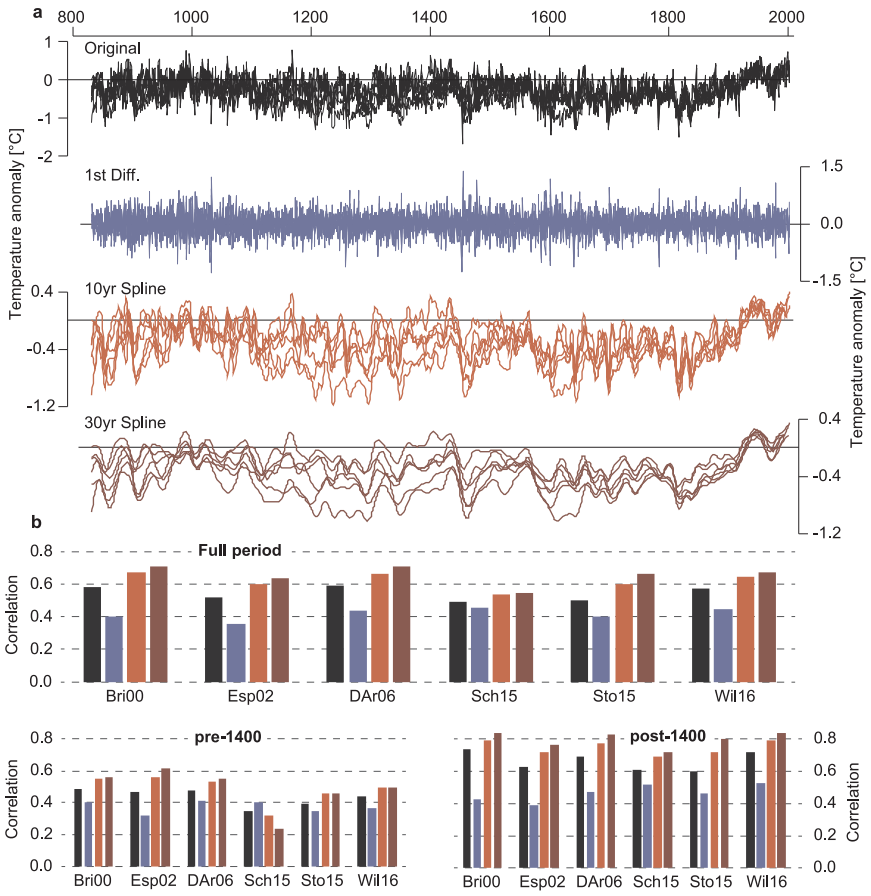

Fig. 5. Reconstruction co-variance. **a**, Six large-scale reconstructions scaled against 30–70 °N JJA temperatures from 1881 to 1992 (black curves), after additional first differencing (blue), 10-year low pass filtering (red), and 30-year low pass filtering (dark red). **b**, Average correlation of each reconstruction with the five other reconstructions using the original (black), first differenced (blue), 10-year smoothed (red), and 30-year smoothed data (dark red). Top panel shows the results calculated over the full (1000–1992) period, bottom left over the early (pre-1400) period, and bottom right over the late (post-1400) period.

alterations between reduced and increased variances after 1400 CE, whereas pre-1400 variance changes are less pronounced and non-synchronous among the reconstructions.

Distinct variance increases are recorded during the 15th century coinciding with severe cooling centered around the 1452 eruption (Esper et al., 2017), an extended period spanning the early 1600 s including the 1600 Huaynaputina eruption (De Silva and Zielinski, 1998), and the late 18th and early 19th centuries centered around the Dalton minimum and 1815 Tambora eruption (Oppenheimer, 2003; Raible et al., 2016; Stothers, 1984). Alternating periods with reduced and increased variance are most pronounced and coherent among the recently published Sch15, Sto15 and Wil16 reconstructions (bottom panel of Fig. 4a) correlating at $r_{1401\text{-}1992} = 0.53$ ($p < 0.1$) but fade before 1400 CE during which cross-reconstruction variance coherence drops to $r_{831\text{-}1400} = 0.06$. The attenuated variance changes and reduced synchronicity among state-of-the-art reconstructions prior to 1400 point to either fewer volcanic eruptions forcing severe large-scale climate perturbations (though the Samalas eruption in 1257 and other large eruptions are reported; Guillet et al., 2017; Lavigne et al., 2013; Vidal et al., 2016) and/or a potential weakening of climatic signal strength of the large-scale reconstructions (see Goosse (2017) and Phipps et al. (2013) for climate model comparisons). The latter could be related to the substantially reduced replication back in time limiting the tree-ring networks' skill to retain large-scale synchronous temperature deviations.

If we consider the first-differenced reconstructions (Fig. 4b), two additional characteristics become apparent: *(i)* an offset between those reconstructions that are either more or less variable, and *(ii)* a drift in variance exhibited by the older reconstructions Bri00 and DAr06. The latter is a bias related to the decline in sample replication and (to a lesser degree) increase in interseries correlation back in time (Osborn et al., 1997). This bias was originally inherent to all early reconstructions (Bri00, DAr06, Esp02), but was adjusted for Esp02 in a follow-up paper addressing artificial variance changes (Frank et al., 2007b). The first-differenced reconstructions also reveal persistent variance offsets, as indicated by standard deviations averaged over the common period since 831 CE ranging from 0.17 °C in DAr06 to 0.36 °C in Sto15 (middle panel in Fig. 4b). Inter-annual temperature variability in the Sch15 and Sto15 records clearly exceeds the variance in all other reconstructions, which is likely related to their use of MXD data, and methodological emphasis placed on high frequency variability to evaluate post-volcanic cooling events in Sto15.

The specific temperature variances displayed here are related to the chosen scaling procedure from 1881 to 1992 against 30–70 °N June-August land temperatures. The absolute values would change if a different season (e.g. annual instead of June-August temperatures), area (e.g., 40–90 °N instead of 30–70 °N), target dataset (e.g. Best instead of CRU temperatures; Harris et al., 2014; Rohde et al., 2013), or method (e.g. regression instead of scaling; Esper et al., 2005) were used, as is the case in the original publications. However, to ensure a direct comparison, as done here, the reconstructions need to be scaled or regressed to a common instrumental target (Harris et al., 2014). The data overlap among the reconstructions and reuse of site chronologies also reinforce a uniform calibration procedure.

The hemispheric scale temperature reconstructions share large fractions of variance in common (Fig. 5). The average correlations between a single reconstruction and all other records calculated over the 831–1992 period range from r = 0.49 (Sch15) to r = 0.59 (DAr06) and are driven by shared reconstructed temperature variances and data overlap among the tree-ring networks. Cross-reconstruction covariance shrinks after first-differencing the records (average $r_{first\text{-}diff.} = 0.35$ to 0.45) but increases after 10-year ($r_{10\text{-}year} = 0.54$ to 0.68) and 30-year ($r_{30\text{-}year} = 0.55$ to 0.71) low pass filtering the records, demonstrating greater similarity at decadal and inter-decadal frequencies. Covariance

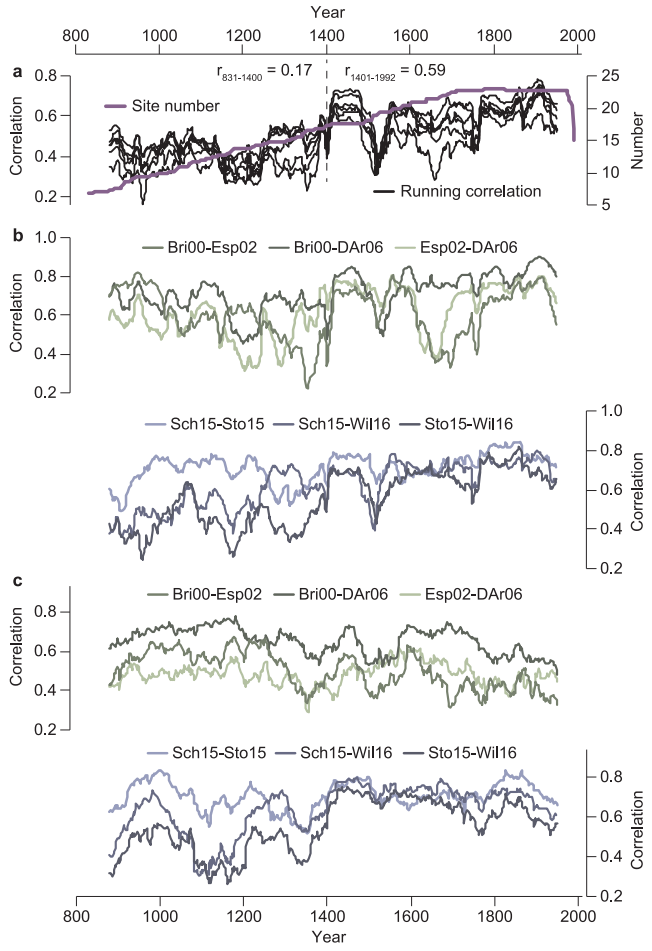

Fig. 6. Reconstruction co-variance. **a**, 100-running correlations among large-scale temperature reconstructions. Each black curve represents the mean derived from correlating one record against its five counterparts. The purple curve is the average number of site chronologies (or clusters) combined in the reconstructions from 831–1992. **b**, Running correlations between the early records (Bri00, Esp02, DAr06) in green and between the recently published records (Sch15, Sto15, Wil16) in blue. **c**, Same as in **b**, but for the first differenced records.

is, however, systematically increased in all frequencies over the recent ~600 years since 1400 CE compared to ~600 years prior 1400 CE during which the correlations among the original records drop from $r_{post\text{-}1400}$ = 0.60 to 0.74, to $r_{pre\text{-}1400}$ = 0.35 to 0.49 (bottom panels in Fig. 5).

This temporal change in inter-reconstruction coherence is also evident in the 100-year running covariance curves calculated over the past millennium (Fig. 6). Again, major volcanic eruptions, such as the 1452 event, increased reconstruction covariance during certain periods, but the most striking feature is a common covariance drop before 1400 CE. This decline from $r_{post\text{-}1400}$ = 0.59 to $r_{pre\text{-}1400}$ = 0.17 reflects a generally weakened reconstruction skill due to constantly shrinking sample replications (purple curve in Fig. 6a). The covariance drop is pronounced between certain reconstruction pairs (e.g. Bri00-Esp02, Sto15-Wil16), whereas other combinations appear to be less affected (Fig. 6b-c). Particularly Sch15-Sto15 co-vary persistently throughout the last millennium reflecting the result of using the same MXD data in both reconstructions. The Bri00-DAr06 pair correlates particularly strong after first-differencing (Fig. 6c) revealing coherent covariance in the high-frequency domain.

5. Last millennium temperature estimates

Even though the hemispheric scale temperature reconstructions express large fractions of common variance, particularly after 1400 CE and at decadal to multi-decadal frequencies, subtle differences in temperature histories exist between these estimates (Fig. 7). Whereas all reconstructions show the 20th was the warmest century over the past 1100 years, the centuries indicated as the very coldest in each record include the 13th (in one reconstruction), 17th (in three) and 19th (in two). The warmest pre-instrumental centuries include the 10th (in one reconstruction), 11th (in three), 14th (in one), and 16th (in one). Focusing on the recently published and much better replicated records, the results are more coherent with respect to the coldest centuries (17th and 19th), but substantial differences remain between the warmest centuries. Particularly the warm 14th century reconstructed by Sch15 provides a new perspective on pre-instrumental climate variability not reflected in any other reconstruction. In Sch15 the transition from the MWP into the LIA is substantially delayed and the LIA temporally constrained to 17th to 19th centuries.

The range of temperatures between the coldest and warmest centuries is largest in Esp02 ($\Delta t_{century}$ = 0.95 °C) and smallest in Sto15 ($\Delta t_{century}$ = 0.33 °C; Fig. 7b). Compared to this substantial dissimilarity at the centennial scale, the temperature ranges between the coldest and warmest 30-year periods are more balanced among the reconstructions ($\Delta t_{30\text{-}year}$ from 0.70 to 1.15 °C). Interestingly, the annual temperature ranges are small in the reconstructions displaying large centennial scale variances (e.g. Esp02 Δt_{annual} = 1.73 °C) and are large in the reconstructions displaying small centennial scale variances (e.g. Sto15 Δt_{annual} = 2.44 °C), i.e. Δt_{annual} is inversely associated with $\Delta t_{century}$ (bottom panel in Fig. 7b). The $\Delta t_{century}/\Delta t_{annual}$ ratio generally shrinks from the earlier (Bri00, Esp02, DAr06) to the newer reconstructions (Sch15, Sto15, Wil16) demonstrating that high frequency temperature variance is emphasized in the state-of-the-art records incorporating more MXD data. This conclusion is in line with earlier observations on increased lag-1 autocorrelation of the older reconstructions (see above, Section 3) and increased first-difference variances in Sch15 and Sto15 (Section 4).

The differences in high frequency variability also influence the estimates of post-volcanic cooling derived from the large-scale reconstructions (Fig. 8). The earlier reconstructions (Bri00, Esp02, DAr06) depict smaller and less distinct cooling in the years following 34 and eight major volcanic eruptions of the past millennium, compared to Sch15, Sto15 and Wil16. The muted signal in the early reconstructions is due to the dominance of TRW data that has been shown to underestimate the magnitude and overestimate the persistence of post-volcanic cooling events (Esper et al., 2015). On the other hand, the new reconstructions all display similar post-volcanic cooling patterns exceeding −0.63 °C (−0.14 °C) in the first year after eight (34) eruptions of the last millennium, even though lag-1 autocorrelation in Sto15 deviates from all other reconstruction and the instrumental target data (Fig. 3), and first-difference variance in Sto15 and Sch15 is persistently larger throughout the past millennium than in any other record including Wil16 (Fig. 4). The Wil16 reconstruction operates in-between these extremes, as it matches the autocorrelation of large-scale summer temperatures and contains high frequency variance comparable to the TRW based reconstructions. It depicts post-volcanic cooling similar to the Sch15 and Sto15 reconstructions in the first post-eruption year, but subsequent recovery is substantially slower.

6. Conclusions and recommendations

Since the late 1990 s, substantial improvements have been made in our understanding of warm season temperature changes over the past millennium. Whereas the first generation of large-scale reconstructions (Bri00, Esp02 and DAr06) explained only a small fraction of hemispheric scale temperature variance, performing least well in the high-

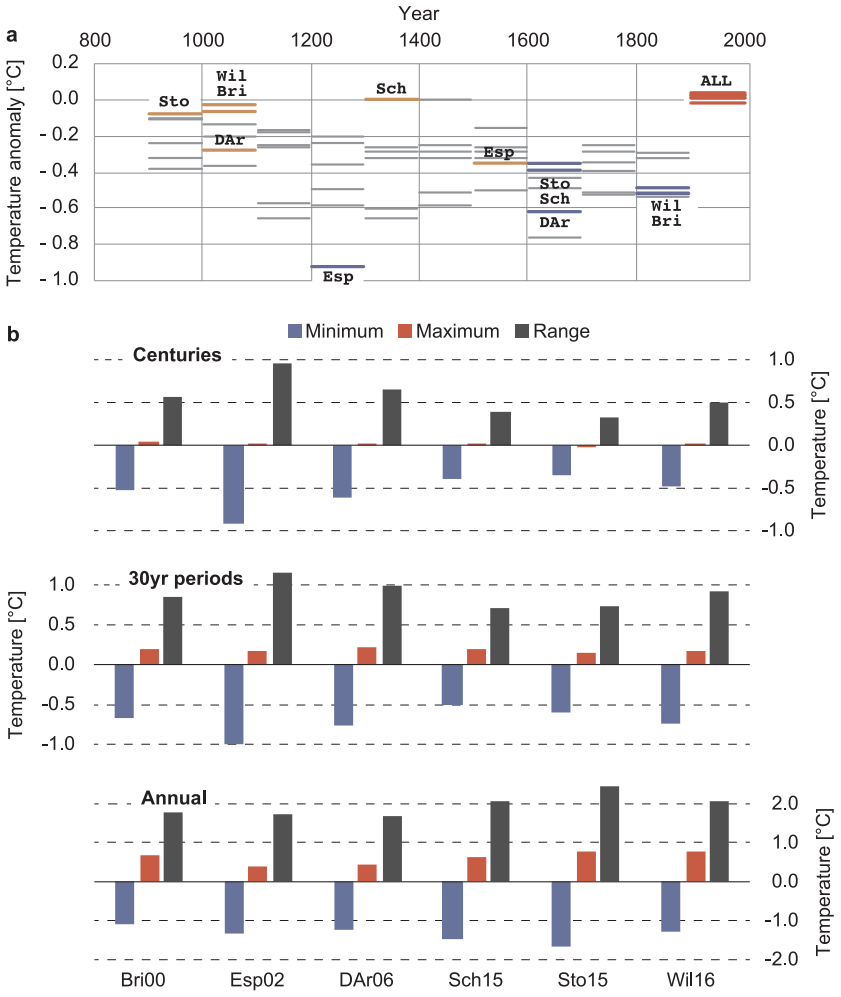

Fig. 7. Reconstructed temperature ranges. **a**, Centennial scale temperature estimates of six tree-ring based reconstructions since 900 CE. Blue bars indicate the coldest reconstructed century for each reconstruction, orange bars the warmest pre-1900 centuries, and red bars the overall warmest century (20th century in all reconstructions). Grey bars are all other centennial values. **b**, Top panel shows the JJA temperature of the coldest (blue) and warmest (red) century, as well as the range between these extremes (black) for each reconstruction. Middle and bottom panels show the same values for 30-year periods and single years.

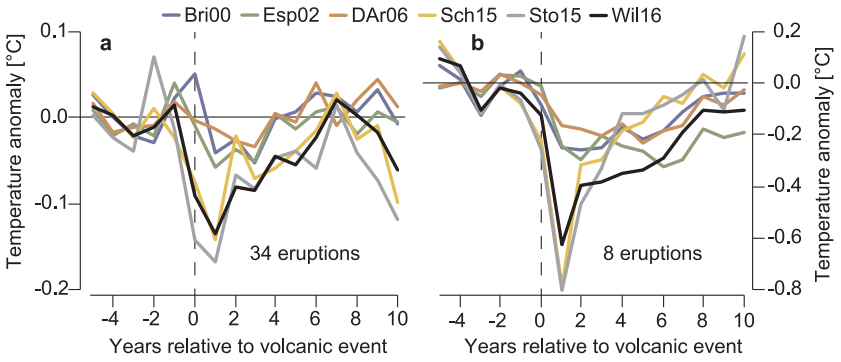

Fig. 8. Post-volcanic cooling patterns in large scale temperature reconstructions. **a**, JJA temperature deviations 5 years before and 10 years after 34 large volcanic eruptions (VEI ≥ 4) of the past millennium (Esper et al., 2013). **b**, Same as in **a**, but using the eight major eruptions listed in Esper et al. (2017).

frequency domain, the new reconstructions published since 2015 (Sch15, Sto15, Wil16) calibrate much better, accounting for ~50% of large-scale summer temperature variance, and now also contain some skill in the inter-annual frequency domain (~30% explained variance). These improvements result from integrating additional MXD chronologies in the tree-ring networks (particularly in Sch15 comprising only MXD) and from expanding the networks and thereby improving the spatial coverage of the NH extratropics (particularly in Sto15 and Wil16). However, the imbalance between well-replicated recent centuries, including the 20th century calibration period, and much weaker replicated early centuries of the last millennium remains also in the newer reconstructions. The substantially reduced replication prior to 1400 CE also appears to be the main reason for the drop in cross-reconstruction covariance, which demonstrates our understanding of large-scale temperature variability during MWP and the transition into the LIA is still limited. The pre-1400 covariance loss is also surprising given the fact that some of the very longest site chronologies (e.g. Torneträsk from northern Sweden) are reused in all reconstructions,

thus increased coherence is to be expected further back in time when replication fades. Efforts to estimate signal changes due to (tree and radii) replication changes in large-scale reconstructions remain a key challenge in dendroclimatic research.

This being said, the three recently published reconstructions – Sch15, Sto15 and Wil16 – represent a major advancement for high resolution paleoclimatology. All three reconstructions are recommended to be used for assessments of warm seasons temperature changes at different temporal scales, though a simple average is not advisable due to the temporally varying overlap in data among the records. One major difference between the three state-of-the-art reconstructions are the much warmer reconstructed 14th century temperatures in the purely MXD based Sch15 reconstruction. To assess whether this new feature, which delays the transition into the LIA by ~100-200 years, is robust, requires further research and the development of even better replicated tree-ring networks covering the last millennium. At inter-annual timescales, the new reconstructions reveal similar post-volcanic cooling patterns, even though we found indication for increased first-differenced variance in Sch15 and Sto15, and limited 20th century autocorrelation in Sto15.

Based on this assessment and comparison of tree-ring based large-scale temperature reconstructions, four research priorities are listed that will likely improve our understanding of high-resolution climate variability of the last millennium:

(1) Update site chronologies to cover most recent decades. Many of the site chronologies included in the NH networks were developed in the 1980 s and 1990 s, precluding calibration tests of the proxy data during the most rapidly warming recent decades.
(2) Develop more temperature sensitive chronologies covering the full millennium. The substantial loss of reconstruction covariance prior to 1400 CE indicates a weakening of climatic signal strength, which is likely related to fewer site chronologies and fewer trees per site chronology covering the MWP and transition into the LIA.
(3) Produce more MXD chronologies. The inclusion of more MXD chronologies has improved the skill of the recently developed reconstructions, particularly in the high frequency domain. Further emphasis on this expensive but superior temperature proxy is recommended.
(4) Advance the statistical estimation of the effects of replication changes on reconstruction skill. The change from thousands of tree-ring series covering the recent centuries to a few hundred of series covering the early centuries of the past millennium requires further assessment. The new papers (Sch15, Sto15, Wil16) include approaches to achieve this objective, but the measurement series included in the networks need to entirely be made available to compare and improve these methods.

Acknowledgements

We are grateful to Keith Briffa for his pioneering work on large-scale temperature reconstructions. Supported by the German Science Foundation, grants # Inst 247/665-1 FUGG and ES 161/9-1. SSG acknowledges support by the Alexander von Humboldt Foundation, KJA by the US National Science Foundation grants AGS-1501856 and NSF AGS-1501834, and JL and LS by the Belmont Forum and JPI-Climate, Collaborative Research Action INTEGRATE. A data file (NH-reconstructions.xlsx) containing the six annually resolved millennial-length reconstructions, scaled over 1881–1992 to June-August 30–70 °N land temperatures, is available at: https://www.blogs.uni-mainz.de/fb09climatology/publications-jan-esper-2/

References

Anchukaitis, K.J., et al., 2012. Tree rings and volcanic cooling. Nat. Geosci. 5, 836–837.
Anchukaitis, K.J., et al., 2017. Last millennium Northern hemisphere summer temperatures from tree rings: part II, spatially resolved reconstructions. Quat. Sci. Rev. 163, 1–22.
Böhm, R., Auer, I., Brunetti, M., Maugeri, M., Nanni, T., Schöner, W., 2001. Regional temperature variability in the European Alps: 1760–1998 from homogenized instrumental time series. Int. J. Climatol. 21, 1779–1801.
Böhm, R., Jones, P.D., Hiebl, J., Frank, D., Brunetti, M., Maugeri, M., 2010. The early instrumental warm-bias: a solution for long central European temperature series 1760–2007. Clim. Change 101, 41–67.
Bothe, O., et al., 2015. Continental-scale temperature variability in PMIP3 simulations and PAGES 2k regional temperature reconstructions over the past millennium. Clim. Past 11, 1673–1699.
Briffa, K.R., 2000. Annual climate variability in the Holocene: interpreting the message of ancient trees. Quat. Sci. Rev. 19, 87–105.
Briffa, K.R., Osborn, T.J., 2002. Blowing hot and cold. Science 295, 2227–2228.
Briffa, K.R., Schweingruber, F.H., Jones, P.D., Osborn, T.J., Shiyatov, S.G., Vaganov, E.A., 1998. Reduced sensitivity of recent tree-growth to temperature at high northern latitudes. Nature 391, 678–682.
Büntgen, U., et al., 2015. Tree-ring amplification of the early nineteenth-century summer cooling in Central Europe. J. Clim. 28, 5272–5288.
Christiansen, B., Ljungqvist, F.C., 2011. Reconstruction of the extratropical NH mean temperature over the last millennium with a method that preserves low-frequency variability. J. Clim. 24, 6013–6034.
Christiansen, B., Ljungqvist, F.C., 2012. The extra-tropical Northern Hemisphere temperature in the last two millennia: reconstructions of low-frequency variability. Clim. Past 8, 765–786.
Christiansen, B., Ljungqvist, F.C., 2017. Challenges and perspectives for large-scale temperature reconstructions of the past two millennia. Rev. Geophys. 55, 40–96.
Cook, E.R., Briffa, K.R., Jones, P.D., 1994. Spatial regression methods in dendroclimatology: a review and comparison of two techniques. Int. J. Climatol. 14, 379–402.
Cook, E.R., Krusic, P.J., Anchukaitis, K.J., Buckley, B.M., Nakatsuka, T., Sano, M., 2013. Tree-ring reconstructed summer temperature anomalies for temperate East Asia since 800 CE. Clim. Dyn. 41, 2957–2972.
Crowley, T.J., Lowery, T.S., 2000. How warm was the medieval warm period? Ambio 29, 51–54.
Crutzen, P.J., 2002. Geology of mankind. Nature 415, 23.
D'Arrigo, R., Wilson, R., Jacoby, G., 2006. On the long-term context for late twentieth century warming. J. Geophys. Res. 111. http://dx.doi.org/10.1029/2005JD006352.
D'Arrigo, R., Wilson, R., Liepert, B., Cherubini, P., 2008. On the 'divergence problem' in northern forests: a review of the tree-ring evidence and possible causes. Glob. Plan. Change 60, 289–305.
D'Arrigo, R., Wilson, R., Anchukaitis, K.J., 2013. Volcanic cooling signal in tree ring temperature records for the past millennium. J. Geophys. Res. Atmos. 118, 9000–9010.
De Silva, S.L., Zielinski, G.A., 1998. Global influence of the AD 1600 eruption of Huaynaputina, Peru. Nature 393, 455–458.
Esper, J., Frank, D.C., 2009. Divergence pitfalls in tree-ring research. Clim. Change 94, 261–266.
Esper, J., Cook, E.R., Schweingruber, F.H., 2002. Low-frequency signals in long tree-ring chronologies and the reconstruction of past temperature variability. Science 295, 2250–2253.
Esper, J., Frank, D.C., Wilson, R.J.S., Briffa, K.R., 2005. Effect of scaling and regression on reconstructed temperature amplitude for the past millennium. Geophys. Res. Lett. 32. http://dx.doi.org/10.1029/2004GL021236.
Esper, J., Schneider, L., Krusic, P.J., Luterbacher, J., Büntgen, U., Timonen, M., Sirocko, F., Zorita, E., 2013. European summer temperature response to annually dated volcanic eruptions over the past nine centuries. Bull. Volcanol. 75. http://dx.doi.org/10.1007/s00445-013-0736-z.
Esper, J., Düthorn, E., Krusic, P., Timonen, M., Büntgen, U., 2014. Northern European summer temperature variations over the Common Era from integrated tree-ring density records. J. Quat. Sci. 29, 487–494.
Esper, J., Schneider, L., Smerdon, J., Schöne, B., Büntgen, U., 2015. Signals and memory in tree-ring width and density data. Dendrochronologia 35, 62–70.
Esper, J., et al., 2016. Ranking of tree-ring based temperature reconstructions of the past millennium. Quat. Sci. Rev. 145, 134–151.
Esper, J., Büntgen, U., Hartl-Meier, C., Oppenheimer, C., Schneider, L., 2017. Northern Hemisphere temperature anomalies during the 1450s period of ambiguous volcanic forcing. Bull. Volcanol. 79 (41). http://dx.doi.org/10.1007/s00445-017-1125-9.
Fernández-Donado, L., et al., 2013. Temperature response to external forcing in simulations and reconstructions of the last millennium. Clim. Past 9, 393–421.
Frank, D., Esper, J., 2005. Temperature reconstructions and comparisons with instrumental data from a tree-ring network for the European Alps. Int. J. Climatol. 25, 1437–1454.
Frank, D., Büntgen, U., Böhm, R., Maugeri, M., Esper, J., 2007a. Warmer early instrumental measurements versus colder reconstructed temperatures: shooting at a moving target. Quat. Sci. Rev. 26, 3298–3310.
Frank, D., Esper, J., Cook, E.R., 2007b. Adjustment for proxy number and coherence in a large-scale temperature reconstruction. Geophys. Res. Lett. 34. http://dx.doi.org/10.1029/2007GL030571.
Frank, D., Esper, J., Zorita, E., Wilson, R.J.S., 2010. A noodle, hockey stick, and spaghetti plate: a perspective on high-resolution paleoclimatology. Wiley Interdisc. Rev. Clim. Change 1, 507–516.
Goosse, H., 2017. Reconstructed and simulated temperature asymmetry between continents in both hemispheres over the last centuries. Clim. Dyn. 48, 1483–1501.
Grudd, H., 2008. Torneträsk tree-ring width and density AD 500-2004: a test of climatic sensitivity and a new 1500-year reconstruction of north Fennoscandian summers.

Clim. Dyn. 31, 843–857.
Guillet, S., et al., 2017. Climate response to the Samalas volcanic eruption in 1257 revealed by proxy records. Nat. Geosci. 10, 123–128.
Harris, I., Jones, P.D., Osborn, T.J., Lister, D.H., 2014. Updated high-resolution grids of monthly climatic observations – the CRU TS3.10 dataset. Int. J. Climatol. 34, 623–642.
Hartl-Meier, C.T.M., Büntgen, U., Smerdon, J.E., Zorita, E., Krusic, P.J., Ljungqvist, F.C., Schneider, L., Esper, J., 2017. Temperature covariance in tree ring reconstructions and model simulations over the past millennium. Geophys. Res. Lett. 44, 9458–9469.
Hegerl, G.C., Crowley, T.J., Allen, M., Hyde, W.T., Pollack, H.N., Smerdon, J., Zorita, E., 2007. Detection of human influence on a new, validated 1500-year temperature reconstruction. J. Clim. 20, 650–666.
Jones, P.D., Briffa, K.R., Barnett, T.P., Tett, S.F.B., 1998. High-resolution palaeoclimatic records for the last millennium: interpretation, integration and comparison with general circulation model control-run temperatures. Holocene 8, 455–471.
Jones, P., et al., 2009. High-resolution paleoclimatology of the last millennium: a review of current status and future prospects. Holocene 19, 3–49.
Juckes, M.N., Allen, M.R., Briffa, K.R., Esper, J., Hegerl, G.C., Moberg, A., Osborn, T.J., Weber, S.L., 2007. Millennial temperature reconstruction intercomparison and evaluation. Clim. Past 3, 591–609.
Lamb, H.H., 1972. Climate: present, past and future. Fundamentals and Climate Now, vol. 1. Methuen, London, pp. 613.
Lavigne, F., et al., 2013. Source of the great AD 1257 mystery eruption unveiled, Samalas volcano, Rinjani Volcanic Complex, Indonesia. PNAS 110, 16742–16747.
Liedtke, H., 1981. Die nordischen Vereisungen in Mitteleuropa. Forschungen zur deutschen Landeskunde 204, 160.
Ljungqvist, F.C., 2010. A new reconstruction of temperature variability in the extra--tropical Northern Hemisphere during the last two millennia. Geografiska Ann. 92, 339–351.
Ljungqvist, F.C., Krusic, P.J., Sundqvist, H.S., Zorita, E., Brattström, G., Frank, D., 2016. Northern Hemisphere hydroclimate variability over the past twelve centuries. Nature 532, 94–98.
Loehle, C., 2007. A 2000-year global temperature reconstruction based on non-treering proxies. Energ. Environ. 18, 1049–1058.
Luterbacher, J., et al., 2016. European summer temperatures since Roman times. Environ. Res. Lett. 11. http://dx.doi.org/10.1088/1748-9326/11/2/024001.
Mann, M.E., Jones, P.D., 2003. Global surface temperatures over the past two millennia. Geophys. Res. Lett. 30. http://dx.doi.org/10.1029/2003GL017814.
Mann, M.E., Bradley, R.S., Hughes, M.K., 1999. Northern hemisphere temperatures during the past millennium: inferences, uncertainties, and limitations. Geophys. Res. Lett. 26, 759–762.
Mann, M.E., Zhang, Z., Hughes, M.K., Bradley, R.S., Miller, S.K., Rutherford, S., Ni, F., 2008. Proxy-based reconstructions of hemispheric and global surface temperature variations over the past two millennia. PNAS 105, 13252–13257.
Melvin, T.M., Grudd, H., Briffa, K.R., 2013. Potential bias in 'updating' tree-ring chronologies using regional curve standardization: reprocessing the torneträsk maximum-latewood-density data. Holocene 23, 364–373.
Moberg, A.D., Sonechkin, M., Holmgren, K., Datsenko, N.M., Karlén, W., 2005. Highly variable Northern Hemisphere temperatures reconstructed from low- and high-resolution proxy data. Nature 433, 613–617.
Neukom, R., Gergis, J., 2012. Southern Hemisphere high-resolution palaeoclimate records of the last 2000 years. Holocene 22, 501–524.
Neukom, R., et al., 2014. Inter-hemispheric temperature variability over the past millennium. Nat. Clim. Change 4, 362–367.
Oppenheimer, C., 2003. Climatic, environmental and human consequences of the largest known historic eruption: Tambora volcano (Indonesia) 1815. Progr. Phys. Geogr. 27, 230–259.
Osborn, T.J., Biffa, K.R., Jones, P.D., 1997. Adjusting variance for sample-size in tree-ring chronologies and other regional-mean timeseries. Dendrochronologia 15, 89–99.
PAGES 2k Consortium, 2013. Continental-scale temperature variability over the Common Era. Nat. Geosci. 6, 339–346.
Parker, D.E., 1994. Effects of changing exposure of thermometers at land stations. Int. J. Climatol. 14, 1–31.
Phipps, S.J., et al., 2013. Paleoclimate data–model comparison and the role of climate forcings over the past 1500 years. J. Clim. 26, 6915–6936.
Qian, W.H., Hu, Q., Zhu, Y.F., Lee, D.K., 2003. Centennial-scale dry-wet variations in East Asia. Clim. Dyn. 21, 77–89.
Raible, C.C., et al., 2016. Tambora 1815 as a test case for high impact volcanic eruptions: earth system effects. Wires Clim. Change 7, 569–589.
Rohde, R., et al., 2013. A new estimate of the average earth surface land temperature spanning 1753 to 2011. Geoinfor. Geostat. Overv. 1. http://dx.doi.org/10.4172/2327-4581.1000101.
Rohling, E.J., 2017. The Oceans: A Deep History. Princeton University Press, Princeton, pp. 272.
Schneider, L., Smerdon, J., Büntgen, U., Wilson, R., Myglan, V.S., Kirdyanov, A., Esper, J., 2015. Revising midlatitude summer temperatures back to AD 600 based on a wood density network. Geophys. Res. Lett. 42. http://dx.doi.org/10.1002/2015GL063956.
Schweingruber, F.H., Bartholin, T., Schär, E., Briffa, K., 1988. Radiodensitometric-dendroclimatological conifer chronologies from Lapland (Scandinavia) and the Alps (Switzerland). Boreas 17, 559–566.
Shi, F., Yang, B., Mairesse, A., Von Gunten, L., Li, J., Bräuning, A., Yang, F., Xiao, X., 2013. Northern Hemisphere temperature reconstruction during the last millennium using multiple annual proxies. Clim. Res. 56, 231–244.
Siddall, M., Rohling, E.J., Almogi-Labin, A., Hemleben, C., Meischner, D., Schmelzer, I., Smeed, D.A., 2003. Sea-level fluctuations during the last glacial cycle. Nature 423, 853–858.
Smerdon, J.E., Pollack, H.N., 2016. Reconstructing earth's surface temperature over the past 2000 years: the science behind the headlines. Wiley Interdisc. Rev. Clim. Change 7, 746–771.
Stoffel, M., et al., 2015. Estimates of volcanic-induced cooling in the Northern Hemisphere over the past 1,500 years. Nat. GeoSci. 8. http://dx.doi.org/10.1038/NGEO2526.
Stothers, R.B., 1984. The great Tambora eruption in 1815 and its aftermath. Science 224, 1191–1198.
van Engelen, A.F.V., Buisman, J., Ijnsen, F., 2001. A millennium of weather, winds and water in the low countries. In: Jones, P.D., Davies, T.D., Ogilvie, A.E.J., Briffa, K.R. (Eds.), History and Climate: Memories of the Future? Kluwer, Dordrecht, pp. 101–124.
Vidal, C.M., Métrich, N., Komorowski, J.C., Pratomo, I., Michel, A., Kartadinata, N., Robert, V., Lavigne, F., 2016. The 1257 Samalas eruption (Lombok, Indonesia): the single greatest stratospheric gas release of the Common Era. Sci. Rep. 6. http://dx.doi.org/10.1038/srep34868.
Wilson, R.J.S., et al., 2016. Last millennium Northern Hemisphere summer temperatures from tree rings. Part I: the long term context. Quat. Sci. Rev. 134, 1–18.
Xing, P., Chen, X., Luo, Y., Nie, S., Zhao, Z., Huang, J., Wang, S., 2016. The extratropical Northern Hemisphere temperature reconstruction during the last millennium based on a novel method. PLoS One 11. http://dx.doi.org/10.1371/journal.pone.0146776.